Dyes and Pigments 184 (2021) 108857

Contents lists available at ScienceDirect

Dyes and Pigments

journal homepage: http://www.elsevier.com/locate/dyepig

Benzannulation via the use of 1,2,4-triazines extends aromatic system of cyclometallated Pt(II) complexes to achieve candle light electroluminescence

Piotr Pander [a,*], Graeme Turnbull [b], Andrey V. Zaytsev [b], Fernando B. Dias [a], Valery N. Kozhevnikov [b,**]

[a] Department of Physics, Durham University, South Road, Durham, DH1 3LE, United Kingdom
[b] Department of Applied Sciences, Northumbria University, Ellison Building, Newcastle Upon Tyne, NE1 8ST, United Kingdom

ARTICLE INFO

Keywords:
1,2,4-Triazine
Organometallics
Platinum
OLED

ABSTRACT

This work describes an application of 1,2,4-triazine methodology for the synthesis of novel cyclometallated Pt (II) complexes of CˆN type. It is shown that addition of a cyclopenteno unit into the complex structure not only facilitates the fabrication of efficient solution-processed OLED devices (EQE_{max} = 10.7%), but also imposes structural changes leading to even more soluble derivatives. Finally, it was shown that by varying the number of fused benzene rings in the CˆN ligand it is possible to tune the emission from green-blueish (Φ_{PL} = 0.15–0.43) to yellow-orange (Φ_{PL} = 0.25). 1,2,4-Triazine methodology gives unique opportunity to fuse additional benzene ring into the pyridine ring and provided the ligand L5 that contained previously unexplored large aromatic system. It was shown that such benzannulation is an effective way to achieve redshift in emission and give rise to solution-processable, single dopant OLED device showing emission spectrum resembling candle light.

1. Introduction

Luminescent cyclometallated Ir(III) and Pt (II) complexes of 2-phenylpyridines and their analogues underpin the development of many fields, ranging from organic light-emitting diodes (OLEDs) to bio-imaging and solar energy conversion [1]. By far the most popular methodology to make such ligands is based on palladium-catalysed cross-coupling reactions as well as traditional pyridine syntheses such as the Kroehnke reaction. For many years, we and others have been exploiting another useful methodology for polypyridine-type ligand synthesis that is based on the use of 1,2,4-triazines as intermediates. In this methodology, 1,2,4-triazines are constructed and then converted to pyridines by means of an inverse electron demand Diels-Alder (IEDDA) reaction. During the IEDDA step of the methodology a variety of substituents can be introduced that allow tuning of physical and photophysical properties of the targeted metal complexes. During IEDDA the N (1) and N (2) atoms of the 1,2,4-triazine are lost and only the N (4) atom remains in the final ligand, therefore cyclometallating aromatic rings have to be introduced either in 3- or in 5- position of 1,2,4-triazines [2]. By using this methodology, structures not accessible by any other methods can be prepared thus providing additional flexibility for the ligand design [3–6].

Pt (II) complexes have a long history of application as emissive materials in OLEDs [7–11]. The square-planar geometry of Pt (II) complexes, however, can cause low solubility of the complexes and therefore causes difficulties in their application to solution-processed devices. The introduction of solubilising groups such as *tert*-butyl groups are often required, however, often at the expense of reduced quantum yields [12]. We have previously shown in several examples that the introduction of cyclopenteno fragment into the pyridine leads to an increase in solubility of the metal complexes without detrimental effect on quantum yield [6]. We therefore prepared a series of four complexes that contain this fragment in the hope that it will assist device fabrication. It should be noted that many more fragments and structural elements can be introduced by the 1,2,4-triazine method. For example, the method is particularly useful for the synthesis of rigid cyclometallating ligands with extended conjugated systems. Delocalised ligands are usually employed to red-shift absorption and emission properties of the

* Corresponding author.
** Corresponding author.
E-mail addresses: piotr.h.pander@durham.ac.uk (P. Pander), valery.kozhevnikov@northumbria.ac.uk (V.N. Kozhevnikov).

https://doi.org/10.1016/j.dyepig.2020.108857
Received 2 June 2020; Received in revised form 28 August 2020; Accepted 11 September 2020
Available online 14 September 2020

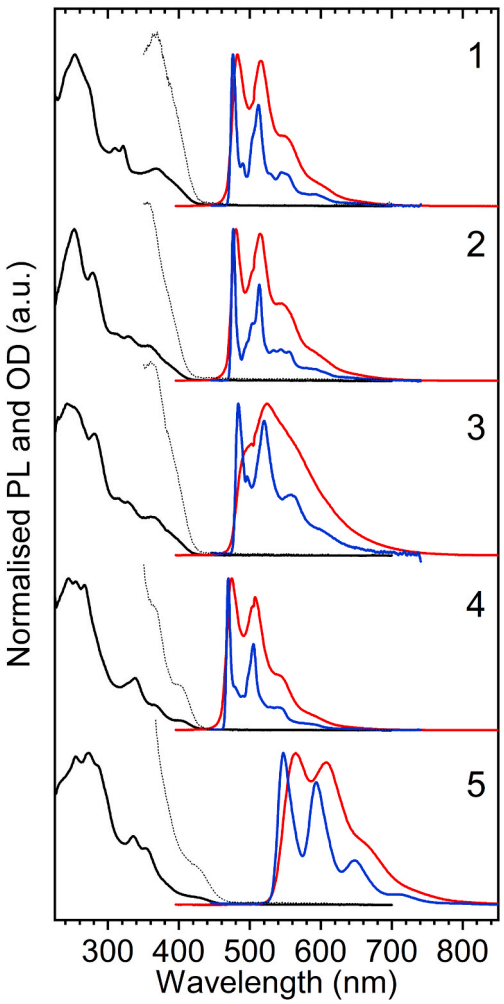

Fig. 1. Absorption (black solid line) and photoluminescence spectra (red: in CH_2Cl_2 at room temperature, blue: 2-MeTHF at 77 K). Black dotted line represents a close-up (x5) of a part of the absorption spectrum near its onset. (For interpretation of the references to colour in this figure legend, the reader is referred to the Web version of this article.)

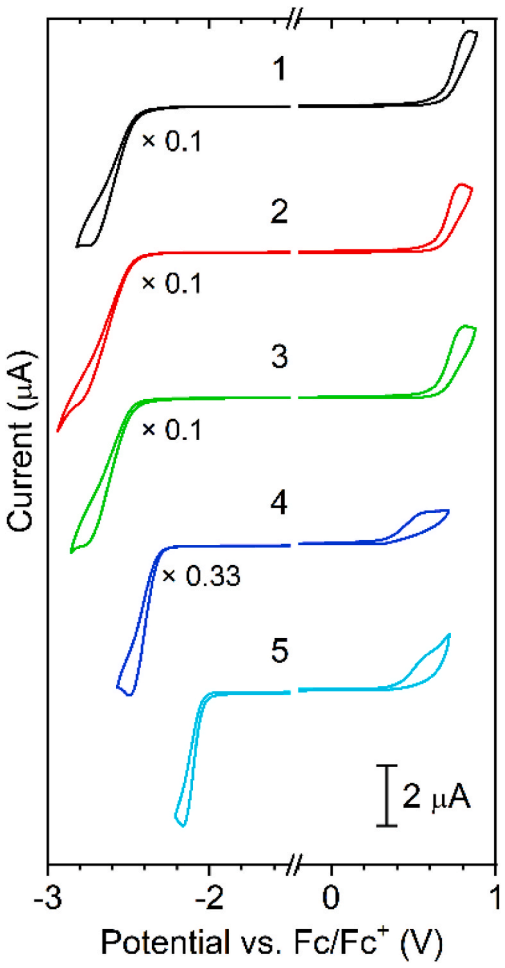

Fig. 2. Electrochemical reduction and oxidation processes recorded using cyclic voltammetry in 0.1 M Bu_4NBF_4/CH_2Cl_2 supporting electrolyte.

corresponding metal complexes [13–15]. However, in some Pt (II) complexes benzannulation can cause both red as well as blue shift of emission [16–18]. For example, Thompson and Yersin investigated in detail the photophysical behaviour of Pt (II) complexes derived from 2-phenylpyridine (ppy), benzo [h]quinoline (bzq) and dibenzo [f, h]-quinoline (dbq) with a progressive increase in the aromatic π-system (Chart 1). A counterintuitive blue shift in emission was registered for the complex derived from dbq that has the largest π-system in the series. Importantly, not only the emission wavelength but also the excited state lifetime is affected by benzannulation. Intrigued by these reports, we decided to investigate the influence of benzannulation of both cyclometallating the aryl as well as the pyridine parts of the ligand. The 1,2,4-triazine methodology provided easy access to the novel ligand **L5** and allows introduction of the annealed benzene ring. In this work we describe the synthesis, photophysical properties and OLED performance of a series of C^N type ligands that contain cyclopenteno fragments as well as the novel highly-conjugated cyclometallating proligand **L5** and its Pt (II) complex **5** designed to achieve red-shifted emission.

2. Materials and methods

Details of photophysical measurements, OLED fabrication and calculations as well as the synthesis of complexes 1–4 are presented in Supporting Information.

Synthesis of phenanthro [9,10-e] -1,2,4-triazine, 9. Formamidinium acetate (1.04 g, 10 mmol) was dissolved in methanol (25 mL). Hydrazine hydrate (485 μL, 500 mg, 10.0 mmol) was added followed by additional methanol (25 mL) and the resulting solution stirred for 5 min 45 mL of this solution was added to a separate reaction mixture containing phenanthrene-9,10-dione (1.50 g, 7.2 mmol) suspended in DMF (20 mL). The mixture was stirred at room temperature for 3 h before the precipitate was collected by filtration, washed with ethanol, and then air dried to give **9** (1.03 g, 50%) as a light brown solid. δ_H (400 MHz, $CDCl_3$) 9.97 (1H, s, Ar–H), 9.47 (2H, d, $J = 8.0$ Hz, 2 x Ar–H), 9.24 (2H, d, $J = 7.6$ Hz, 2 x Ar–H), 8.90 (2H, d, $J = 8.4$ Hz, 2 x Ar–H), 7.85–7.92 (2H, m, 2 x Ar–H), 7.74–7.82 (2H, m, 2 x Ar–H). δ_C (101 MHz, $CDCl_3$) 155.3 (Ar-CH), 147.1 (quat.), 143.3 (quat.), 133.7 (quat.), 132.6 (Ar-CH), 131.3 (quat.), 131.1 (Ar-CH), 128.7 (Ar-CH), 128.2 (Ar-CH), 127.6 (quat.), 127.4 (quat.), 126.6 (Ar-CH), 125.1 (Ar-CH), 123.1 (Ar-CH), 123.0 (Ar-CH). HRMS (ESI) *m/z* 232.08687 ($[M+H]^+$); $C_{15}H_{10}N_3$ requires 232.08692.

Synthesis of cyclopenta [*c*] dibenzo [f,h] quinoline, 10. A mixture of **9** (782 mg, 3.4 mmol) and 1-pyrrolidinocyclohexene (543 mg, 565 μL, 3.6 mmol) was heated at 170 °C for 1.5 h under an argon atmosphere. After this, another portion of 1-pyrrolidino-1-cyclohexene (543 mg, 565 μL, 3.6 mmol) was added and the reaction was allowed to stir at 170 °C for a further 16 h. The reaction mixture was isolated via flash column chromatography using petroleum ether:EtOAc (4:1) as an eluent to yield **10** (775 mg, 81%) as a brown-yellow solid. δ_H (400 MHz, $CDCl_3$) 9.24–9.27 (1H, m, Ar– H), 8.66 (1H, d, $J = 8.4$ Hz, Ar–H), 8.63 (1H, s,

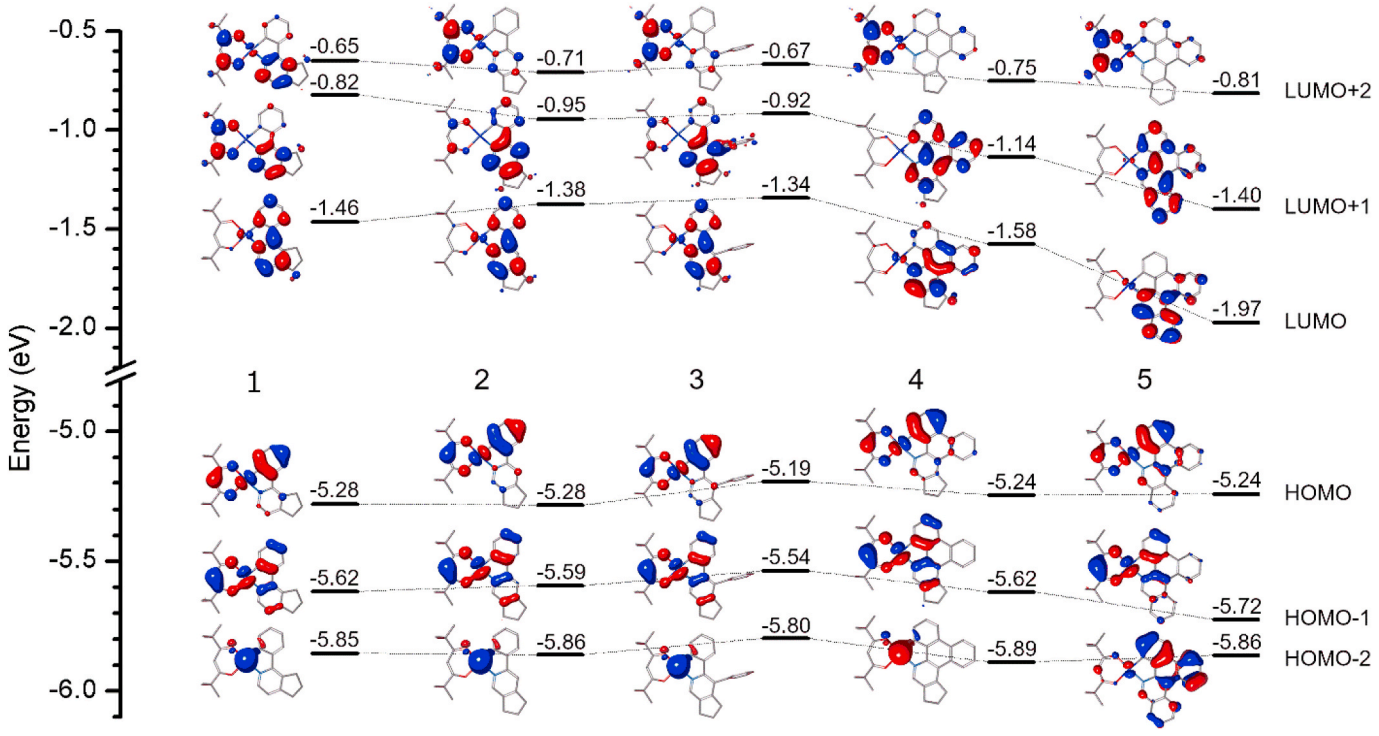

Fig. 3. Selected molecular orbital surfaces and their energy. Iso value: 0.03. Orbital energy depicted in eV.

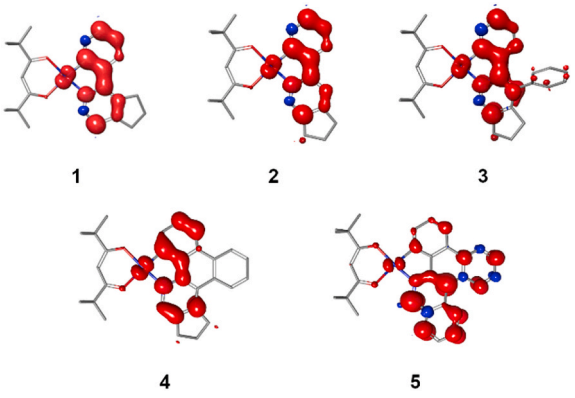

Fig. 4. Spin density of the lowest excited triplet state at T_1 geometry. Iso value: 0.003.

Ar–H), 8.53–8.55 (1H, m, Ar–H), 8.51 (1H, d, J = 8.4 Hz, Ar–H), 7.63–7.70 (3H, m, Ar–H), 7.56 (1H, t, J = 7.6 Hz, Ar–H), 3.43 (2H, app. t, CH_2), 3.04 (2H, app. t, CH_2), 1.94–2.01 (2H, m, CH_2), 1.74–1.80 (2H, m, CH_2). δ_C (101 MHz, $CDCl_3$) 149.7 (Ar-CH), 149.7 (Ar-CH), 145.1 (quat.), 144.0 (quat.), 131.6 (quat.), 131.2 (quat.), 131.1 (quat.), 130.8 (quat.), 129.5 (quat.), 129.1 (Ar-CH), 128.2 (Ar-CH), 127.4 (Ar-CH), 126.9 (Ar-CH), 125.5 (Ar-CH), 125.3 (Ar-CH), 124.7 (quat.), 123.4 (Ar-CH), 122.1 (Ar-CH), 32.9 (CH_2), 26.9 (CH_2), 23.7 (CH_2), 22.0 (CH_2). HRMS (ESI) m/z 284.14316 ($[M+H]^+$); $C_{21}H_{18}N$ requires 284.14337.

Synthesis of the proligand L5. To a solution of **10** (700 mg, 2.5 mmol) in m-xylene (50 mL) was added DDQ (560 mg, 2.5 mmol) and the reaction mixture heated to reflux under an argon atmosphere for 2 h. A second equivalent of DDQ was added (560 mg, 2.5 mmol) and the reflux continued for a further 2 h. A third equivalent of DDQ was added (560 mg, 2.5 mmol) and reflux continued overnight. The solvent was then removed under reduced pressure and the residue sonicated with DCM (40 mL) for 5 min. The resulting precipitate was collected by filtration and washed with small amount of DCM. The filtrate was evaporated and the residue purified by flash column chromatography using petroleum ether:EtOAc (4:1) as the eluent to yield **L5** (205 mg, 30%) as a beige solid. δ_H (400 MHz, $CDCl_3$) 9.45 (1H, s, Ar–H), 9.35–9.38 (1H, m, Ar–H), 8.97 (1H, d, J = 8.8 Hz, Ar–H), 8.93 (1H, d, J = 8.0 Hz, Ar–H), 8.78 (1H, d, J = 8.0 Hz, Ar–H), 8.66–8.69 (1H, m, Ar–H), 8.18 (1H, d, J = 7.6 Hz, Ar–H), 7.85 (1H, app. t, Ar–H), 7.67–7.79 (5H, m, 5 x Ar–H). δ_C (101 MHz, $CDCl_3$) 151.8 (Ar-CH), 141.6 (quat.), 132.6 (quat.), 131.1 (quat.), 130.9 (quat.), 130.7 (quat.), 130.5 (Ar-CH), 128.9 (Ar-CH), 128.7 (quat.), 128.5 (Ar-CH), 128.2 (Ar-CH), 127.5 (Ar-CH), 127.1 (Ar-CH), 126.7 (Ar-CH), 126.6 (Ar-CH), 126.4 (Ar-CH), 125.4 (Ar-CH), 123.6 (Ar-CH), 122.3 (Ar-CH), 119.5 (quat.). HRMS (ESI) m/z 280.11200 ($[M+H]^+$); $C_{21}H_{14}N$ requires 280.11207.

Synthesis of complex 5. A mixture of **L5** (82 mg, 0.29 mmol) and potassium tetrachloroplatinate (110 mg, 0.13 mmol) was added to ethoxyethanol (9 mL) in water (3 mL) and the mixture heated to 90 °C for 24 h. The mixture was cooled, and the resulting precipitate was collected by filtration, washed with water and then methanol and dried in air to yield the intermediate (106 mg). Then a mixture of this intermediate (84 mg, 0.15 mmol), dipivaloylmethane (85 mg, 0.46 mmol), sodium carbonate (163 mg, 1.54 mmol) and ethoxyethanol (4 mL) was stirred at 100 °C for 16 h. The mixture was then cooled to RT, diluted with water, and extracted into diethyl ether (3 × 20 mL). The combined organic layers were dried over $MgSO_4$ and concentrated under reduced pressure. The product was purified by column chromatography on silica using petroleum ether:DCM (7:3) as the eluent to yield 5 (41 mg, 41%) as a bright yellow solid. δ_H (400 MHz, $CDCl_3$) 9.75 (1H, s, Ar–H), 9.00 (1H, d, J = 8.8 Hz, Ar–H), 8.96 (1H, d, J = 8.1 Hz, Ar–H), 8.75 (1H, d, J = 8.0 Hz, Ar–H), 8.24 (1H, d, J = 8.1 Hz, Ar–H), 8.11 (1H, d, J = 7.9 Hz, Ar–H), 7.92 (1H, t, J = 7.8 Hz, Ar–H), 7.86 (1H, d, J = 8.1 Hz, Ar–H), 7.75–7.59 (4H, m, Ar–H), 5.90 (1H, s, =CH), 1.40 (9H, s, $C(CH_3)_3$), 1.36 (9H, s, $C(CH_3)_3$). δ_C (101 MHz, $CDCl_3$) 195.3 (C═O), 193.9 (C═O), 153.3 (Ar-CH), 150.5 (Ar-CH), 140.8 (Ar-CH), 136.4 (Ar-CH), 133.2 (Ar-CH), 132.8 (Ar-CH), 132.7 (Ar-CH), 130.0 (Ar-CH), 130.0 (Ar-CH), 128.9 (Ar-CH), 128.5 (Ar-CH), 128.4 (Ar-CH), 128.3 (Ar-CH), 127.6 (Ar-CH), 127.6 (Ar-CH), 126,9 (Ar-CH), 126.5 (Ar-CH), 126.3 (Ar-CH), 124.2 (Ar-CH), 120.1 (Ar-CH), 116.7 (Ar-CH), 93.5 (CH), 41.7 ($\underline{C}CH_3$),

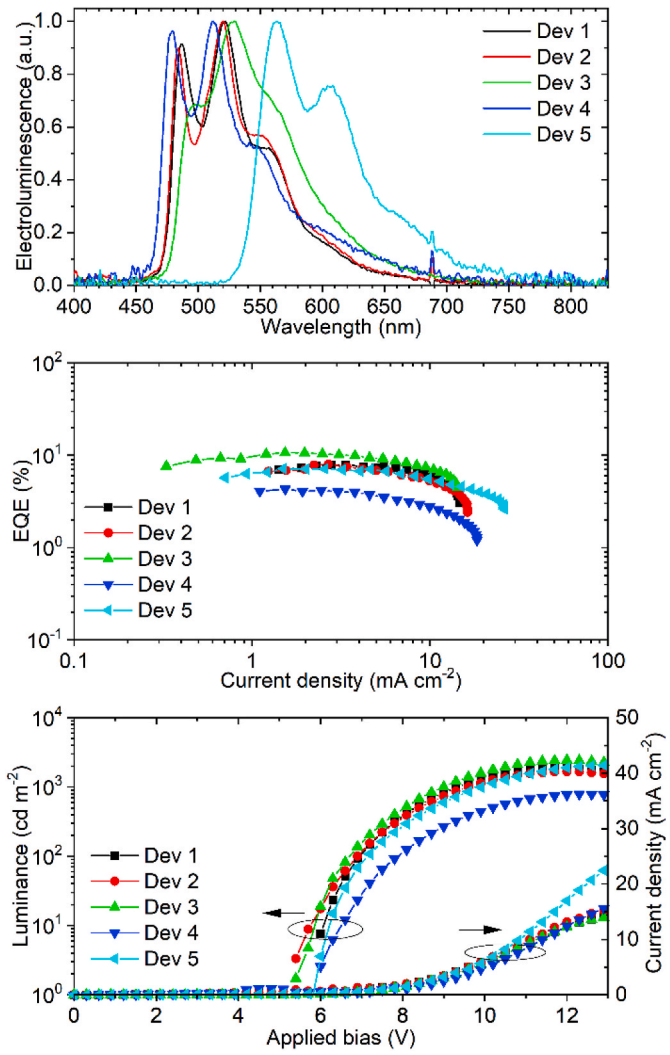

Fig. 5. Summary of OLED characteristics; top: electroluminescence spectra; middle: external quantum efficiency (EQE) *vs*. current density; bottom: luminance & current density *vs*. applied bias.

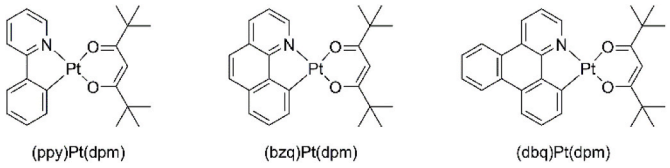

Chart 1. A series of the complexes evaluated by Thompson and Yersin [16].

41.3 ($\underline{C}CH_3$), 28.9 (3 x CH_3), 28.6 (3 x CH_3).

3. Results and discussion

3.1. Synthesis

The synthesis of the target ligands is depicted in Scheme 1. The 1,2,4-triazine starting materials **6,** [2,19] **7** [20], **8** and **9** [21] are prepared according to known procedures. The triazines are then reacted with 1-pyrrolidinocyclopentene to obtain proligands **L1-4** that contain the 3, 4-(cyclopenteno) pyridine fragment (experimental procedures for all cyclopenteno derivatives are available in supporting information). The ligand **L5** can theoretically be obtained from triazine **9** in one step *in-situ* by reaction with the generated benzyne dienophile [22]. However, our attempt to carry out this reaction gave a very low yield. Instead, a two-step procedure was followed in which **9** was first reacted with 1-pyrrolidinocyclohexene to introduce a cyclohexeno fragment, followed by oxidation of **10** with DDQ leading to the aromatic system **L5**. To the best of our knowledge this ligand as well as its metal complexes have not been prepared previously.

Overall all ligands were easy to prepare using inexpensive starting materials and without the use of a Pd catalyst, thus eliminating the problem of removing colloidal Pd metal particles from the final products. This demonstrates another advantage of this 1,2,4-triazine methodology over cross-coupling reactions. Pt (II) complexes **1–5** were prepared by following a known method in which the proligands are first reacted with potassium tetrachloroplatinate to obtain dichloro-bridged intermediates. These are then converted into the desired ligands by treatment with dipivaloylmethane (dpmH) in the presence of potassium carbonate.

3.2. Photophysics

All complexes are emissive in solution and in the solid state (Fig. 1, S1). **1**, **2**, and **4** show similar green-blueish photoluminescence and the vibronic patterns of their emission spectra show clear resemblance. This is despite the ligand of **4** being significantly different from the other two. Complex **3** shows a similar emission onset to **1**, **2**, and **4**, but its photoluminescence spectrum shows a distinctly different vibronic pattern. As shown later through calculations, the T_1 excited state of **3** exhibits a significant degree of distortion, therefore affecting the vibronic structure of the spectrum. This behaviour does not occur in **1** and **2** which retain their ground state geometry in the excited state. Complex **5** shows the most red-shifted, orange-yellow photoluminescence.

All molecules show similar absorption spectra but do not always follow the trend in their emission characteristics. In particular, the absorption onset changes in series **2** (417 nm) < **3** (424 nm) < **1** (429 nm) < **4** (435 nm) < **5** (463 nm) do not correspond directly to the photoluminescence onset values **4** (457 nm) < **2** (465 nm) ≈ **1** (465 nm) < **3** (471 nm) < **5** (534 nm) in CH_2Cl_2 at room temperature. The same order is maintained at 77 K in 2-MeTHF. This seems to suggest that in **4** the ground state and excited state differ i.e. in the degree of conjugation. In other words, the peripheral phenyl ring is not being involved in the excited state of **4** while it may interact in the ground state. This is shown clearly in calculations as the HOMO and LUMO gap is effectively lower in **4** than in **1** and **2**, due to larger conjugation in the former (Fig. 3). The T_1 state spin density does however reside on the same part of molecule in all three cases, indicating that the outer benzene ring of the **4** ligand does not contribute to the lowest triplet excited state (Fig. 4). Interestingly, while the outer benzene ring does not influence the excited state of **4**, the contribution of this unit is turned on in **5** through addition of a second benzene ring. The reason for the strong photoluminescence and absorption red-shift is therefore the extended conjugation of the phenylpyridine ligand with what is effectively two benzene rings.

Direct S_0-T_1 transitions are not observed in the absorption spectra, indicating a modest oscillator strength and resulting in a small extinction coefficient ($\varepsilon < 100\ M^{-1}cm^{-1}$, Fig. S2). A summary of photophysical characteristics in solution can be found in Table 1, while data for the solid state can be found in the SI (Table S1).

The photoluminescence spectra of all of the presented metal complexes gain a significant degree of vibronic resolution at 77 K in 2-MeTHF, with the most significant change visible in **3**. This suggests that due to its distorted geometry in the T_1 state, **3** shows rapid conformational interconversion that occurs faster than the photoluminescence decay timescale. This process is slowed down at low temperatures (or even completely suppressed), allowing the molecule to emit before completing geometry relaxation.

The photoluminescence decay lifetimes observed for complexes **1**–**4** ($\tau \approx 1$–8 μs) are typical for metal complexes used in OLED applications

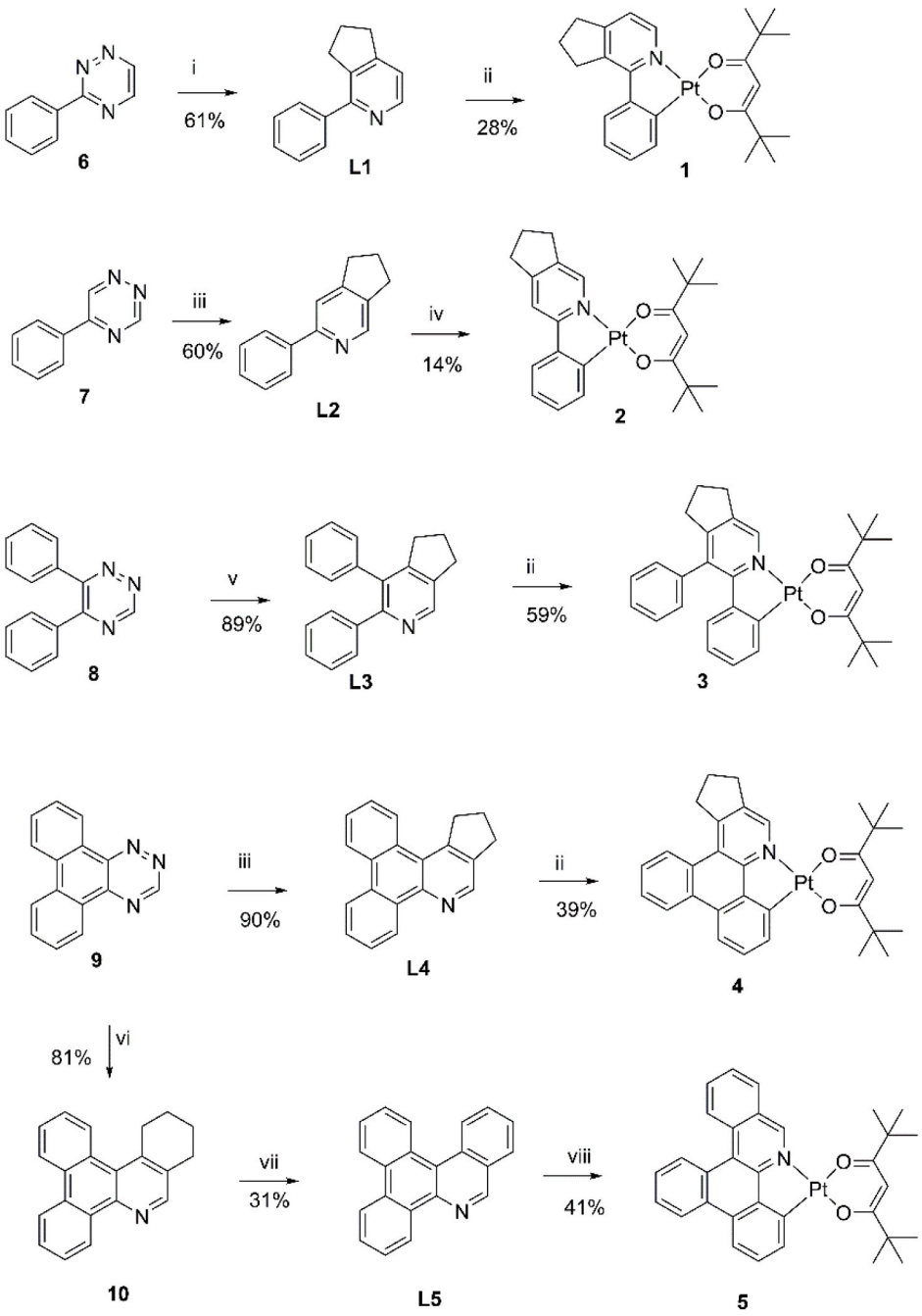

Scheme 1. The use of 1,2,4-triazines in the synthesis of the target proligands and their Pt (II) complexes. Reaction conditions: i) 1) Cyclopentanone, morpholine, molecular sieves, 110 °C, 1 h; 2) AcOH, reflux 30 min; ii)1) K_2PtCl_4, AcOH, reflux; 2) dipivaloylmethane, K_2CO_3, ethoxyethanol, 100 °C, 16–18 h; iii) 1-pyrrolidinocyclopentene, toluene, reflux, 12 h; 2) AcOH, reflux, 15 min; 1) K_2PtCl_4, AcOH, reflux; 2) DMSO, 110 °C, 1 h; 3) dipivaloylmethane, K_2CO_3, ethoxyethanol; v) 1) 1-pyrrolidinocyclopentene, toluene, 60 °C, 1 h; 2) AcOH, reflux, 10 min; vi) 1-pyrrolidinocyclohexene, neat, 170 °C, 16 h; vii) DDQ, m-xylene, reflux, 16 h; viii) K_2PtCl_4, ethoxyethanol/water (3/1, v/v), 90 °C, 24 h; 2) dipivaloylmethane, K_2CO_3, ethoxyethanol, 100 °C, 16 h.

[9,23], however for complex **5** $\tau = 44.7$ μs. Such differences in lifetimes are associated with the degree of $d_{Pt(II)}$ admixture to the triplet excited state. It is a general trend that lowering metal orbital admixtures to the T_1 state results in decrease of the respective radiative rate constants which are expressed as elongated phosphorescence lifetimes [23,24]. All of these Pt (II) complexes show moderate to good photoluminescence quantum yields with the maximum $\Phi_{PL} = 0.43$ observed for **3** and the minimum $\Phi_{PL} = 0.15$ for **4** in diluted CH_2Cl_2 solution. More importantly, despite the introduction of an additional degree of freedom into the complex **3** in the form of an outer phenyl ring, the Φ_{PL} is larger by ≈ 30% than in analogous molecules **1** and **2**. The Φ_{PL} values for complexes **1**, **2**, and **4** are reduced by 10–25% in relation to their analogues without the cyclopenteno unit [16]. The organometallic compounds studied here show an increase of photoluminescence lifetime in 2-MeTHF glass at 77 K. The change is consistent with the radiative and non-radiative rate constants calculated at room temperature (Table 1). Rather surprisingly, **5** remains moderately emissive ($\Phi_{PL} = 0.25$) regardless of its modest radiative rate constant $k_r = 5.7 \times 10^3\ s^{-1}$ being an order of magnitude smaller than in other complexes. This is because the non-radiative rate constant follows the radiative rate and remains small. This however contradicts the typical rule of the energy gap law that predicts the non-radiative rate constant rises with decreased excited state energy [25].

In general, the behaviour of the metal complexes presented in this work in solid films (with the same composition as their respective emissive layers in OLEDs) is similar to that in solution (Fig. S1, Table S1). The photoluminescence spectra, lifetimes and quantum yields of these complexes are similar to those recorded in CH_2Cl_2 solutions. The one significant difference is that photoluminescence decay in the solid state at both room temperature and 77 K remain biexponential, while all

Table 1
Summary of spectroscopic and electrochemical characteristics.

Complex		1	2	3	4	5
Absorption at 295 K	λ_{max}, nm (ε, M^{-1} cm^{-1})[a]	400sh (2800), 369 (6100), 321 (9700), 310 (9400), 253 (24,900)	390sh (2400), 359 (6100), 328 (7800), 312 (8200), 278 (19,000), 252 (26,700)	400sh (2200), 360 (5800), 327 (8000), 314 (8500), 280 (18,200), 242 (22,700)	401 (2300), 368 (6000), 338 (13,100), 267 (36,300), 253 (37,200), 245 (38,200)	430sh (1800), 350 (15,400), 336 (18,800), 274 (41,100), 254 (40,200)
	E_g^{opt}, eV [b]	2.94	2.99	2.95	2.90	2.71
Emission at 295 K[n]	**λ_{max}, nm** [c]	482, 516, 551sh, 603sh	480, 514, 541, 600sh	490sh, 523	474, 507, 544sh, 593sh	565, 608, 677sh
	T, μs [d]	2.8	4.1	7.4	1.6	44.7
	Φ_{PL} [e]	0.31	0.27	0.43	0.15	0.25
	$k_r \times 10^{-3}$, s^{-1} [f]	111	65	58	93	5.7
	$\Sigma k_{nr} \times 10^{-3}$, s^{-1} [g]	250	180	76	540	17
Emission at 77 K[o]	**λ_{max}, nm** [c]	476, 490sh, 504sh, 512, 530sh, 544, 554sh, 594sh	476, 496sh, 503sh, 513, 533, 543, 555, 595sh	484, 496, 520, 558, 605sh	469, 479, 496sh, 505, 528, 541sh, 586sh	547, 594, 647, 711sh
	T, μs [d]	7.8	9.7	8.9	7.2	82.3
	T_1, eV [h]	2.64	2.63	2.61	2.67	2.35
Cyclic voltammetry	**E_{ox}^{onset}, V** [i]	0.67	0.63	0.64	0.36	0.40
	E_{red}^{onset}, V [j]	≈ −2.45	≈ −2.45	≈ −2.45	−2.32	−2.05
	IP, eV [k]	5.77	5.73	5.74	5.46	5.50
	EA, eV [l]	≈2.65	≈2.65	≈2.65	2.78	3.05
	E_g^{el}, eV [m]	≈3.1	≈3.1	≈3.1	2.68	2.45

[a] Absorption maxima with respective molar absorption coefficient in parentheses.
[b] Optical energy gap recorded from absorption spectrum onset, $1240\lambda_{onset}^{-1}$.
[c] Photoluminescence maxima.
[d] Photoluminescence lifetime recorded at emission maximum wavelength.
[e] Photoluminescence quantum yield.
[f] Radiative rate constant.
[g] Sum of non-radiative rate constants.
[h] Lowest triplet state energy recorded from phosphorescence spectrum onset, $1240\lambda_{onset}^{-1}$.
[i] Onset oxidation potential.
[j] Onset reduction potential.
[k] Ionisation energy, $IP = E_{ox}^{onset} + 5.1$ (eV).
[l] Electron affinity, $EA = E_{red}^{onset} + 5.1$ (eV).
[m] Electrochemical energy gap, $E_g^{el} = IP\text{-}EA$.
[n] Recorded in degassed CH_2Cl_2 at room temperature.
[o] Recorded in 2-methyltetrahydrofuran (degassed) glass at 77 K. Emission spectra and TCSPC traces recorded at 10^{-5} M concentration of complex.

measurements recorded in solution indicate a monoexponential decay (see Figs. S3–S7 for decay in solution and Figs. S8–S12 for decay in thin film). This is likely due to inhomogeneity of the films and is a common behaviour. To facilitate comparison between the photoluminescence lifetime in solution and in the solid state a weighted average lifetime is used in the latter case [26]. There is significantly less difference between a solid state complex's properties at room temperature and 77 K than there is in solution. This is because there is less vibrational/rotational freedom for the molecule in solid films even at room temperature and this does not change significantly at lower temperatures. Furthermore, as expected in a polymer matrix, the host is not completely frozen at 77 K and this allows for much more freedom to the molecules than a 2-MeTHF glass at same temperature. This is manifested as only a small improvement of the vibrational resolution in photoluminescence spectra *vs*. room temperature. Importantly, the emission spectra of **3**-doped films remain nearly the same at both room temperature and 77 K.

3.3. Electrochemistry

The electrochemical behaviour of all complexes shows good correlation with their photophysical properties in the ground state as corresponding electrochemical and optical energy gaps follow the same trend (Fig. 2). Electrochemical processes reveal how a ground state molecule reacts in a chemical reaction involving the receipt or donation of electrons. The electrical potential at which these processes occur can be transposed to an energy scale representing the HOMO and LUMO levels of the molecule (as their approximation), or more precisely their ionisation potential (IP) and electron affinity (EA), respectively [27,28].

The ground state behaviour seen in electrochemistry will reflect the degree of conjugation present in the complex. In the case of molecules **1**, **2** and **3** their respective oxidation and reduction potentials are nearly identical. This clearly suggests that their conjugation is limited to the phenylpyridine moiety and it does not extend to the peripheral phenyl ring in **3**. The outer phenyl group is thus orthogonal to the rest of the phenylpyridine ligand. This view is also supported by computational analysis (Fig. 3, S16).

Complex **4** shows very different electrochemical properties from **1** and **2** despite all three having nearly identical emission spectra. This is because in the ground state of **4** the outer benzene ring is conjugated, at least partly, with the phenylpyridine moiety. This results in a narrower electrochemical energy gap by reducing the oxidation potential and increasing the reduction potential. In the excited state however, the peripheral phenyl ring does not play a significant role (Fig. 4). Finally, a further extension of the ground state conjugation is observed in **5**, showing the smallest electrochemical energy gap. **5** however, clearly shows a red-shifted emission from other emitters, especially **4**.

3.4. Calculations

In order to understand the different emissive behaviour of the investigated organometallic compounds, basic quantum mechanical calculations have been performed. In the ground state all complexes but **5** are planar around the Pt (II) centre and within the π-conjugated system of ligands, while only the aliphatic groups remain off-plane (Fig. 3 and S13-S17). **5** however shows its extended phenylpyridine ligand to be twisted (see ESI, Fig. S18). This helicene-like twist is caused by repulsion of hydrogen atoms in adjacent benzene rings of the ligand π-conjugated structure. All geometries calculated at the lowest triplet excited state, except for **3** and **5**, are in general almost identical to the ground state structures. In case of **3** in the T_1 state the C–C bond axis connecting the single phenyl substituent is distorted out of plane along with the rest of the phenylpyridine ligand (Fig. S16). This behaviour explains the different vibronic pattern of the emission spectrum in **3** compared to the analogues **1** and **2**.

To characterise $T_1 \rightarrow S_0$ transitions the T_1 was calculated at the T_1 geometry to reflect changes to the structure in the excited state. Due to fast intersystem crossing the excited S_n states at the S_1 state geometry are not discussed as they are of negligible importance for this study.

In all cases the lowest singlet excitation is related predominantly to the HOMO→LUMO transition with the same dominant contribution of LUMO→HOMO in the $T_1 \rightarrow S_0$ transition (Table S2). However, HOMO-1→LUMO and HOMO-2→LUMO transitions also contribute to the singlet and triplet excitations. Interestingly, the contribution of the HOMO→LUMO transition to the lowest singlet excitation in **5** is the largest among all at 95% while the value for complexes **1**–**3** remains at ≈85%. Excitation energies and the energies of triplet excited states clearly follow the trends observed in experimental data. $S_0 \rightarrow S_1$ energy at S_0 geometry shows good agreement with the experimental absorption spectra, however the $S_0 \rightarrow T_1$ energy at T_1 geometry shows a systematic 0.3–0.4 eV offset from the experiment. These calculations clearly explain the emissive properties of the complexes. In all compounds the HOMO and the LUMO both span over the π-conjugated system of the ligands with both having pronounced metal orbital admixtures. Apart from contributions of the central atom to both frontier orbitals, the HOMO spans over the dpm ligand and the phenyl arm of the extended phenylpyridine ligand, while the LUMO spans almost exclusively on the extended phenylpyridine ligand. This behaviour reflects the relative electron-deficient and electron-rich regions of the molecule. The HOMO and LUMO surfaces and spin density distribution in T_1 state for complexes **1**, **2**, and **4** presented in this work show perfect resemblance to their analogues studied by Bossi et al. [16].

Analysis of the spin density of the T_1 state calculated at the lowest triplet excited state geometry is crucial for understanding the emissive properties of **4** *vs*. **1** and **2**, but also gives an important insight into the properties of **5** (Fig. 4). Generally speaking, the T_1 spin density spans over the extended phenylpyridine ligand unit with a sound contribution of the metal centre. However, the distribution of the spin density in **4** is nearly identical to that of **1** and **2**. This again indicates that in fact the outer phenyl ring in **4** does not take part in emission, limiting the conjugation to the phenylpyridine itself. Interestingly, substitution of the cyclopentene ring by the benzene ring in **5** not only extends spin density over that unit but also turns on the contribution of the other outer benzene ring that is not contributing to the spin density in **4**. The turn-on of the second benzene unit fully explains the strong redshift of photoluminescence emission in **5**. Extension of the π-conjugated system achieved in **5** effectively destabilises the quinoid conjugation of the T_1 state of molecules **1**–**4** towards benzenoid conjugation in complex **5**.

3.5. Devices

The T_1 energy of all complexes but **5** is relatively large, close to 2.7 eV, with the emission onset entering the blue spectral region [29]. For this reason a host comprised of poly (*N*-vinylcarbazole) (PVK) and 1, 3-bis [2-(4-*tert*-butylphenyl)-1,3,4-oxadiazo-5-yl]benzene (OXD-7) (50:50 w/w) is used as this mixture has previously shown good performance in blue PhOLED devices based on FIrPic-like metalorganic emitters [30]. The use of OXD-7 in relation to the popular 2-(biphenyl-4-yl)-5-(4-*tert*-butylphenyl)-1,3,4-oxadiazole (PBD) is necessary due to the low triplet energy of the latter which quenches high energy triplet states of emitters. The use of the PVK:OXD-7 blend for all molecules is justified by the need for consistency, as by using the same host it is easier to make comparisons between emitters. 1,3,5-tri (*m*-pyridin-3-ylphenyl) benzene (TmPyPb) is used as an electron transport layer. A simple device structure has been employed, without the use of hole transport/electron blocking layers: ITO | Heraeus Clevios HIL 1.3 N (45 nm) | PVK:OXD-7 (50:50 w/w) co. 5% (wt.) emitter (70 nm) | TmPyPb (50 nm) | LiF (0.8 nm) | Al (100 nm). In general, using a high molecular weight PVK, $M = 1.1 \times 10^6$ g mol^{-1}, (PVKH) layer (10 nm thick) in between hole injection layer (HIL) and emissive layer (EML) gives a good charge balance [31–33], however, this approach can only be used with EML solution-processed from non-chlorinated solvents, such as toluene. Due to the limitations in solubility of OXD-7 as well as the

Table 2
Summary of OLED device characteristics.

Device		Dev 1	Dev 2	Dev 3	Dev 4	Dev 5
Emitter		1	2	3	4	5
V_{ON} (at 10 cd m^{-2}), V [a]		6.1	5.8	5.8	6.5	6.2
L_{max}, cd m^{-2} [b]		1870	1680	2440	790	2030
λ_{max}, nm [c]		487, 521, 554sh, 605sh	483, 520, 555sh, 610sh	498, 529, 563sh	479, 512, 550sh	563, 606, 660sh
CIE 1931 (x; y) [d]		0.26; 0.56	0.27; 0.55	0.33; 0.57	0.26; 0.49	0.52; 0.47
$H_{L, max}$, cd A^{-1} [e]		24.5	23.0	34.4	11.3	19.6
$H_{ext., max}$, % [f]		7.9	8.0	10.7	4.3	7.1
2 mA cm^{-2}	**η_L, cd A^{-1}** [g]	22.2	19.6	34.2	11.2	19.6
	$H_{ext.}$, % [h]	6.9	6.9	10.5	4.2	6.9
10 mA cm^{-2}	**η_L, cd A^{-1}** [g]	18.5	15.4	23.5	7.0	14.5
	$H_{ext.}$, % [h]	5.9	5.2	7.1	2.8	5.6
$J_{90\%}$, mA cm^{-2} [i]		7.0	4.0	4.0	4.5	6.5

[a] Turn-on voltage at 10 cd m^{-2}.
[b] Maximum luminance.
[c] Electroluminescence spectrum maxima.
[d] Colour coordinates at maximum luminance as defined in International Commission on Illumination colour space CIE 1931.
[e] Maximum current efficiency.
[f] Maximum external quantum efficiency ±10% error.
[g] Current efficiency at specified current density.
[h] External quantum efficiency at specified current density.
[i] Current density at 90% $\eta_{ext., max}$ ±0.5 mA cm^{-2} [39].

emitters, especially **4**, in toluene, a mixture of chloroform:chlorobenzene (95:5 v/v) was used as a solvent [34].

In general, the limited solubility of **4** led to an emitter load of only 5% wt. This load usually gives promising results with a variety of emitters, while lower loads, such as 1–3% may cause incomplete energy transfer from host to guest, thus reduced efficiency [12,31,32]. Again, the same load was used for all other molecules, regardless of their better solubility. To compensate the lack of hole transport layer (HTL), the EML is made relatively thick (70 nm). This approach to device structure has proven to be very successful in solution-processed devices based on Pt (II) and Ir(III) organic complexes [12,35,36].

The devices show a turn on at ≈5–5.5 V achieving brightness of 10 cd m^{-2} at ≈ 6 V which is a rather typical value in this type of device structure, suggesting a satisfactory alignment of energy levels (Table 2). The electroluminescence spectrum is generally consistent with photoluminescence spectra in both solid and solution states (Fig. 5). Devices using **1**, **2**, and **4** show a green-blueish electroluminescence with the bluest being the **4**-based, CIE 1931 (0.26; 0.49). The **3**-based device shows green electroluminescence, while the OLED using **5** shows yellow-orange emission, CIE (0.52; 0.47) that resembles candlelight, CIE (0.52, 0.42) [12,37,38]. Maximum device efficiency ($\eta_{ext., max}$) generally follows the trend of Φ_{PL} in solid film, assuming 0.2–0.3 outcoupling factor and applying measurement uncertainties. The highest $\eta_{ext., max}$ achieved in a device using **3** as an emitter was 10.7 ± 1.1%, with maximum luminance reaching 2440 cd m^{-2}. Modest device luminance of less than 2500 cd m^{-2} can be attributed to relatively low current density, that is below 25 mA cm^{-2} for all devices.

Interestingly, efficiency roll-off is comparable in all devices and typical for the type of emitter used [39], even in the device using **5** as an emitter and despite it having the longest phosphorescence lifetime in solid film, 64 ± 3 μs. Complex **5** still shows very good performance, regardless of its long photoluminescence lifetime, about an order of magnitude larger than that of molecules **1**–**4** (Table S1). This behaviour suggests that in the particular current density regime of the presented OLED devices the triplet-quenching processes do not significantly affect the roll-off. Therefore, despite the long-lived phosphorescence, **5** is still suitable to be used in electroluminescent devices.

4. Conclusions

In this work we have described an application of 1,2,4-triazine methodology for the synthesis of novel cyclometallated Pt (II) complexes of CˆN type. It has been shown that the introduction of the cyclopenteno unit does not significantly diminish the quantum yield of the emitters but does influence their geometry. The most striking example is the complex **3**, in which, according to calculations, the outer phenyl ring is nearly perpendicular to the main plane of the complex. Such geometries are desirable to improve solubility as well as to diminish aggregation of the planar Pt (II) complexes and are usually achieved by employing mesitylene (2,4,6-trimethylphenyl) fragments. In case of **3** a similar geometry is enforced by the cyclopenteno fragment. Complex 3 was used to fabricate solution-processed OLEDs that achieve EQE up to 10.7%.

Another successful example of the use of the 1,2,4-triazine methodology is the synthesis of a novel cyclometallating ligand **L5** and its corresponding Pt (II) complex **5**. The benzannulation caused redshifted emission and a large decrease in the radiative rate constant of the photoluminescence. However, Φ_{PL} of complex **5** remains moderate (0.25) and the complex was successfully used to produce OLED with emission that resembles candlelight. The reported proligands may be used in future to prepare cyclometallated Ir(III) and other metal complexes and 1,2,4-triazine methodology is therefore a useful addition to the toolkit of tuning the physical and photophysical properties of cyclometallated metal complexes.

CRediT authorship contribution statement

Piotr Pander: Conceptualization, Writing - original draft, Preparation, Writing - review & editing, Investigation, Data curation, Visualization. **Graeme Turnbull:** Writing - review & editing, Investigation. **Andrey V. Zaytsev:** Writing - review & editing, Investigation. **Fernando B. Dias:** Writing - review & editing, Resources, Funding acquisition. **Valery N. Kozhevnikov:** Conceptualization, Writing - original draft, Preparation, Writing - review & editing, Investigation, Project administration, Funding acquisition.

Declaration of competing interest

The authors declare that they have no known competing financial interests or personal relationships that could have appeared to influence the work reported in this paper.

Acknowledgments

Authors would like to thank EPSRC for funding this research through project Nº EP/S012788/1.

Appendix A. Supplementary data

Supplementary data to this article can be found online at https://doi.org/10.1016/j.dyepig.2020.108857.

References

[1] Djurovich PI, Murphy D, Thompson ME, Hernandez B, Gao R, Hunt PL, Selke M. Dalton Trans 2007:3763.
[2] Neunhoeffer H, Weischedel F. Justus Liebigs Ann Chem 1971;749:16–23.
[3] Pabst GR, Pfüller OC, Sauer J. Tetrahedron 1999;55:8045–64.
[4] Kozhevnikov VN, Ustinova MM, Slepukhin PA, Santoro A, Bruce DW, Kozhevnikov DN. Tetrahedron Lett 2008;49:4096–8.
[5] Santoro A, Prokhorov AM, Kozhevnikov VN, Whitwood AC, Donnio B, Williams JAG, Bruce DW. J Am Chem Soc 2011;133:5248–51.
[6] Kozhevnikov DN, Kozhevnikov VN, Ustinova MM, Santoro A, Bruce DW, Koenig B, Czerwieniec R, Fischer T, Zabel M, Yersin H. Inorg Chem 2009;48:4179–89.
[7] Gildea LF, Williams JAG. Organic light-emitting diodes (OLEDs), vol. 62. Elsevier; 2013. p. 77–113.
[8] Tang M-C, Chan AK-W, Chan M-Y, Yam VW-W. Top Curr Chem 2016;374:46.
[9] Li G, She Y. Light-emitting diode - an outlook on the empirical features and its recent technological advancements. InTech; 2018.
[10] Petrenko A, Leitonas K, Volyniuk D, Baryshnikov GV, Belyakov S, Minaev BF, Ågren H, Durgaryan H, Gražulevičius JV, Arsenyan P. Dalton Trans 2020;49:3393–7.
[11] Arsenyan P, Petrenko A, Leitonas K, Volyniuk D, Simokaitiene J, Klinavičius T, Skuodis E, Lee J-H, Gražulevičius JV. Inorg Chem 2019;58:10174–83.
[12] Pander P, Bulmer R, Martinscroft R, Thompson S, Lewis FW, Penfold TJ, Dias FB, Kozhevnikov VN. Inorg Chem 2018;57:3825–32.
[13] Bura T, Retailleau P, Indelli MT, Ziessel R. Dalton Trans 2013;42:4544–51.
[14] Edkins RM, Fucke K, Peach MJG, Crawford AG, Marder TB, Beeby A. Inorg Chem 2013;52:9842–60.
[15] Howarth AJ, Majewski MB, Wolf MO. Coord Chem Rev 2015;282–283:139–49.
[16] Bossi A, Rausch AF, Leitl MJ, Czerwieniec R, Whited MT, Djurovich PI, Yersin H, Thompson ME. Inorg Chem 2013;52:12403–15.
[17] Mandapati P, Braun JD, Killeen C, Davis RL, Williams JAG, Herbert DE. Inorg Chem 2019;58:14808–17.
[18] Kourkoulos D, Karakus C, Hertel D, Alle R, Schmeding S, Hummel J, Risch N, Holder E, Meerholz K. Dalton Trans 2013;42:13612.
[19] O'Rourke M, Lang SA, Cohen E. J Med Chem 1977;20:723–6.
[20] WO/2019/116037, 2019.
[21] Laakso PV, Robinson R, Vandrewala HP. Tetrahedron 1957;1:103–18.
[22] Gonsalves AMdAR, Pinho e Melo TMVD, Gilchrist TL. Tetrahedron 1992;48:6821–6.
[23] Yersin H. Highly efficient OLEDs with phosphorescent materials. Wiley; 2008.
[24] Kozhevnikov DN, Kozhevnikov VN, Shafikov MZ, Prokhorov AM, Bruce DW, Gareth Williams JA. Inorg Chem 2011;50:3804–15.
[25] Englman R, Jortner J. Mol Phys 1970;18:145–64.
[26] Graves D, Jankus V, Dias FB, Monkman A. Adv Funct Mater 2014;24:2343–51.
[27] Bredas J-L. Mater Horiz 2014;1:17–9.
[28] Cardona CM, Li W, Kaifer AE, Stockdale D, Bazan GC. Adv Mater 2011;23:2367–71.
[29] Lee JH, Cheng SH, Yoo SJ, Shin H, Chang JH, Wu CI, Wong KT, Kim JJ. Adv Funct Mater 2015;25:361–6.
[30] Kozhevnikov VN, Zheng Y, Clough M, Al-Attar HA, Griffiths GC, Abdullah K, Raisys S, Jankus V, Bryce MR, Monkman AP. Chem Mater 2013;25:2352–8.
[31] Shafikov MZ, Daniels R, Pander P, Dias FB, Williams JAG, Kozhevnikov VN. ACS Appl Mater Interfaces 2019;11:8182–93.
[32] Pashazadeh R, Pander P, Lazauskas A, Dias FB, V Grazulevicius J. J Phys Chem Lett 2018;9:1172–7.
[33] Pander P, Gogoc S, Colella M, Data P, Dias FB. ACS Appl Mater Interfaces 2018;10:28796–802.
[34] Colella M, Pander P, Monkman AP. Org Electron 2018;62:168–73.
[35] Tavasli M, Moore TN, Zheng Y, Bryce MR, Fox Ma, Griffiths GC, Jankus V, Al-Attar Ha, Monkman AP. J Mater Chem 2012;22:6419–28.
[36] Benjamin H, Zheng Y, Batsanov AS, Fox MA, Al-Attar HA, Monkman AP, Bryce MR. Inorg Chem 2016;55:8612–27.
[37] Jou J-H, Su Y-T, Liu S-H, He Z-K, Sahoo S, Yu H-H, Chen S-Z, Wang C-W, Lee J-R. J Mater Chem C 2016;4:6070–7.
[38] Jou J-H, Hsieh C-Y, Chen P-W, Kumar S, Hong JH. J Photon Energy 2014;4:043598.
[39] Murawski C, Leo K, Gather MC. Adv Mater 2013;25:6801–27.